A Full-Range and High-Dynamic Control Method of Neutral Point Potential for Parallel Three Level Inverters Considering Zero-Sequence Circulating Current

Zhongrui Li, Ziling Nie, Sheng Ai, Jie Xu, and Huayu Li

***Abstract*—Parallel three-level inverters (PTLIs) are widely used in high-power applications to improve the system capacity and reliability. However, the three-level topology in PTLIs inevitably introduces the imbalance of neutral-point potential (NPP), and the NPP control (NPPC) of PTLIs must consider zero-sequence circulating current (ZSCC). The existence of ZSCC may cause the failure of NPPC methods for a single TLI to be directly applied to PTLIs. To solve this issue, a full-range and high-dynamic control method of NPP for PTLIs considering ZSCC is proposed in this article. First, the independent zero-sequence voltage injection (ZSVI) method is extended to PTLIs with the consideration of ZSCC. Meanwhile, treating PTLIs as one six-phase TLI for NPPC is proposed in this article, and the uniform ZSVI method for PTLIs is analyzed in detail. Based on the uniform ZSVI method, the modulation wave decomposition (MWD) method is implemented to balance NPP in the full modulation index range. Furthermore, to improve the dynamic performance of NPPC, an online neutral compensation current estimation (ONCCE) method combining a proportional regulator and a nonlinear disturbance observer is proposed. Combining the uniform ZSVI, MWD, and ONCCE methods organically, the full-range and high-dynamic NPPC is achieved, and the balance effect, control range, and dynamic performance are obviously improved. The experimental results obtained from an industry prototype of PTLIs verify the effectiveness of the proposed method.**

***Index Terms*—Modulation wave decomposition (MWD), neutral-point potential control (NPPC), online neutral compensation current estimation (ONCCE), parallel three-level inverters (PTLIs), zero-sequence circulating current (ZSCC), zero-sequence voltage injection (ZSVI).**

NOMENCLATURE

FESS	Flywheel energy storage system.
TLI	Three-level inverter.
PTLIs	Parallel three-level inverters.
NPP	Neutral-point potential.
ZSCC	Zero-sequence circulating current.
CMVD	Common-mode voltage difference.
NPPC	Neutral-point potential control.
CBPWM	Carrier-based pulsewidth modulation.
SVPWM	Space vector pulsewidth modulation.
ZSVI	Zero-sequence voltage injection.
MWD	Modulation wave decomposition.
ZSV	Zero-sequence voltage.
NCC	Neutral compensation current.
ONCCE	Online NCC estimation.
NDOB	Nonlinear disturbance observer.
PMSM	Permanent magnet synchronous motor.
TLI-k	kth TLI of PTLIs.
v_x, i_x	Reference voltage and phase current of PTLIs.
v_{xk}, i_{xk}	Reference voltage and phase current of TLI-k.
$i_{\rm o}$, $v_{\rm o}$	Neutral current and ZSV of PTLIs.
$i_{{\rm o}k}$, $v_{{\rm o}k}$	Neutral current and ZSV of TLI-k.
$i_{\rm NCC}$	NCC of PTLIs.
$u_{\rm o}$	NPP of PTLIs.
$v_{{\rm cm}k}$, L_k	Common-mode voltage and inductor of TLI-k.
$i_{{\rm z}k}$, m_k	ZSCC and amplitude ratio of TLI-k.
$i_{\rm d}$, $i_{\rm de}$	Total disturbance and its estimated value.
$i_{\rm dn}$, $i_{\rm du}$	Effects of nonlinearities and external uncertainties on NCC.
$C_{\rm H}$, $C_{\rm L}$,	Dc-link Capacitors.
C, ΔC	Capacitance and capacitance variation.
$u_{\rm cH}$, $u_{\rm cL}$	Capacitor voltages.
$U_{\rm dc}$	Dc-bus voltage.
$k_{\rm p}$, δ	Proportional and NDOB gains.
m, $I_{\rm m}$	Modulation index and phase current amplitude.
ω, φ	Angular frequency and power factor angle.
$T_{\rm s}$, $f_{\rm r}$	Switching period and fundamental frequency.
$d_{xk{\cdot}{\rm o}}$	Zero duty cycle.
$v_{xk{\cdot}{\rm p}}$, $v_{xk{\cdot}{\rm n}}$	Positive and negative reference voltages.
$u_{\rm obH}$, $u_{\rm obL}$	Upper and lower limits of the activation band.
$*$	Reference value.

Manuscript received 12 July 2023; revised 19 September 2023; accepted 17 October 2023. Date of publication 20 October 2023; date of current version 6 December 2023. This work was supported by the National Natural Science Foundation of China under Grant 52077219. Recommended for publication by Associate Editor M. Narimani. *(Corresponding author: Sheng Ai.)*

The authors are with the State Key Laboratory of Electromagnetic Energy, Naval University of Engineering, Wuhan 430033, China (e-mail: lzrui@zju.edu.cn; nzl23@nue.edu.cn; aisheng23@nue.edu.cn; baboo_x23@nue.edu.cn; lihuayu23@nue.edu.cn).

Color versions of one or more figures in this article are available at https://doi.org/10.1109/TPEL.2023.3326307.

Digital Object Identifier 10.1109/TPEL.2023.3326307

I. INTRODUCTION

IN RECENT years, there has been an increasing demand for high-power inverters in certain industrial applications.

For example, FESS has received extensive attention due to the ability of storing and releasing massive energy with high power (MW) during short periods (seconds) [1]. Since the inverter is an essential part of FESS, it also requires high-power operation.

For high-power applications, compared with conventional two-level inverters (TLIs), TLIs have the advantages of high voltage level, low harmonic content, and high working efficiency [2], [3], which are more attractive and widely employed. Besides, to overcome the current capacity limitation of a single TLI, parallel operation is a practical alternative solution. PTLIs can extend the current capacity, increase the power rating, and improve the system reliability [4], [5], the topology of which has been widely used in high-power applications such as renewable energy generation, photovoltaic grid connection, and energy storage systems [6], [7], [8]. However, an inherent issue of PTLIs is NPP imbalance, including dc-imbalance, and ac-imbalance due to the dc bias and ac fluctuation of capacitor voltages. The NPP imbalance can overstress devices, increase harmonics, and reduce efficiency, affecting the safe and efficient operation of PTLIs [9]. Besides, the ZSCC inevitably emerges due to the excitation of CMVD in PTLIs [10], which has an undeniable effect on NPP and causes the inability of NPPC methods for a single TLI to be directly applied to PTLIs.

Numerous NPPC methods for a single TLI have been proposed in the literature, which can be classified as SVPWM and CBPWM methods. The conventional SVPWM performs NPPC by distributing the dwell time of redundant small vectors [11], [3], which can control the dc-imbalance of NPP, but cannot completely eliminate the ac-imbalance under high modulation index and low power factor. The virtual SVPWM can achieve the full-range control of NPP [12], [13], but the switching loss is increased due to extra virtual vectors. The hybrid SVPWM combining the conventional SVPWM and the virtual SVPWM can simultaneously control NPP in full range and reduce switching losses [14], [15]. However, all SVPWM methods require complex sector division and duty cycle calculation, making it difficult to extend to PTLIs because with the number of TLIs increases, the number of voltage vectors also increases sharply, which seriously increases the computational burden.

Compared with SVPWM methods, CBPWM methods are easier to implement, including the ZSVI, MWD and hybrid methods. In [16] and [17], the ZSVI method is used for three-phase and dual three-phase TLIs, achieving NPPC by injecting an optimal ZSV calculated with interpolation. Although the ZSVI method is simple and convenient to implement, it cannot completely eliminate the ac-imbalance of NPP just like the conventional SVPWM method. To control ac-imbalance of NPP in full range, the MWD method is proposed in [18] and [19] for three-phase and multiphase TLIs, which decomposes one modulation wave per phase into two modulation waves and adjusts the neutral current with three-level switching in each period. However, extra switching actions significantly increase switching losses and worsen harmonic characteristics. Combining ZSVI and MWD, lots of hybrid methods are proposed. In [2], a hybrid method based on proportional integral regulator is proposed, which combines ZSVI and MWD organically and activates MWD only when necessary. In [20], the hybrid method performs ZSVI or "ZSVI+MWD" to offer the optimal performance regarding controllability, switching losses, and output harmonics. In [21], a hybrid method with three degrees of freedom is proposed, which can realize the maximum controllability of NPP.

All of these NPPC methods are designed for a single TLI, but the PTLIs cannot be simply treated as a single TLI for NPPC. The effective NPPC of PTLIs needs to consider ZSCC. In [22], a coordinated strategy based on SVPWM is proposed to provide ZSCC suppression and NPPC. In [6], an improved modulation method is proposed, which modifies the dwell time of positive small vectors considering ZSCC suppression and NPPC. However, these researches pay more attention on ZSCC suppression and the effect of ZSCC on NPPC is not considered. Besides, the NPPC methods used are too simple and limited to achieve better range and performance. In this article, the PTLIs applied to FESS is studied. To achieve the effective NPPC of PTLIs, the NPPC methods presented in this article are implemented with the consideration of ZSCC. In these methods, it is found that the balance effect of NPP is sensitive to the accuracy of NCC. In [17], the NCC is obtained from simple calculation. However, the capacitance variation in the operation of PTLIs can affect the calculation of NCC. In practice, parameter inaccuracies and external disturbances can affect the accuracy of NCC and result in poor dynamic performance. To ensure the effective NPPC and obtain the high-dynamic performance, the NCC can be estimated online.

The main contributions of this article are as follows.

1) In PTLIs, the NPPC has to consider the effect of ZSCC. The NPPC methods for a single TLI does not taken this issue into account and cannot be directly applied to PTLIs. To solve this issue, the independent ZSVI method is extended to PTLIs considering ZSCC. Besides, treating the PTLIs as one six-phase TLI to achieve NPPC is proposed in this article, and the uniform ZSVI method is analyzed in detail.
2) For applications of PTLIs with high modulation index, the ZSVI method cannot effectively control the ac-imbalance of NPP. To overcome this limitation, the MWD method for PTLIs is also implemented by treating the PTLIs as one six-phase TLI in this article. The MWD method can achieve a full-range NPPC, meaning it can balance NPP with a modulation index range of 0 to 1.15.
3) The NCC has an obvious effect on the effectiveness of ZSVI and MWD methods. To degrade the effect of parameter inaccuracies and external disturbances on the accuracy of NCC, an ONCCE method combining a proportional regulator and a NDOB, called as "P+NDOB," is proposed to estimate the NCC of PTLIs. The ONCCE method can improve the dynamic performance of NPPC by obtaining an accurate NCC, thereby achieving the high-dynamic NPPC.
4) In order to achieve the full-range NPPC and the high-dynamic NPPC simultaneously, the uniform ZSVI, MWD and ONCCE methods are organically combined in this article.

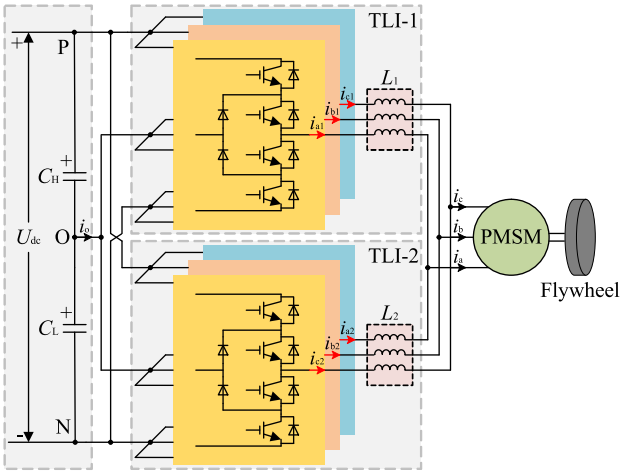

Fig. 1. Topology of PTLIs in FESS.

The rest of this article is organized as follows. Section II analyzes the mechanism of NPP imbalance for PTLIs. Section III discusses the ZSVI methods of PTLIs. Section IV presents the MWD, ONCCE and proposed methods. Section V shows the experimental results. Finally, Section VI concludes this article.

II. Mechanism of NPP Imbalance for PTLIs

Fig. 1 shows the topology of PTLIs in FESS. The PTLIs consists of two TLIs with the same structure, namely TLI-1 and TLI-2. The two TLIs share the same dc-bus and are connected to the PMSM and flywheel through common-mode inductors in the output side. In this figure, $U_{\rm dc}$ is the dc-bus voltage, $C_{\rm H}$ and $C_{\rm L}$ are two dc-link capacitors, L_k ($k=1,2$) is the common-mode inductor, i_{xk} ($x=$ a, b, c) is the phase current of TLI-k, and i_x is the phase current of PTLIs.

Normalized based on $U_{\rm dc}/2$, the reference voltages of PTLIs can be expressed as

$$\begin{cases} v_{\rm a} = m\cos(\omega t) \\ v_{\rm b} = m\cos(\omega t - 2\pi/3) \\ v_{\rm c} = m\cos(\omega t + 2\pi/3) \end{cases} \tag{1}$$

where m is the modulation index of the range [0, 1.15] and ω is the angular frequency. Meanwhile, the phase currents of PTLIs can be expressed as

$$\begin{cases} i_{\rm a} = I_{\rm m}\cos(\omega t - \varphi) \\ i_{\rm b} = I_{\rm m}\cos(\omega t - \varphi - 2\pi/3) \\ i_{\rm c} = I_{\rm m}\cos(\omega t - \varphi + 2\pi/3) \end{cases} \tag{2}$$

where $I_{\rm m}$ is the amplitude of phase currents and φ is the power factor angle, which is typically 0 in FESS with PMSM.

The inverter nonlinear characteristics, such as dead time, can lead to an original common-mode voltage for TLI-k [10]. Normalized based on $U_{\rm dc}/2$, the common-mode voltage is

$$v_{{\rm cm}k} = m_k\cos(3\omega t) \tag{3}$$

where m_k is the amplitude ratio.

Due to parameter differences, the common-mode voltages of TLI-1 and TLI-2 are different, and the CMVD of PTLIs is not zero. According to the relationship between CMVD and ZSCC [10], the ZSCCs of TIL-1 and TIL-2 with the same magnitude and opposite direction can be expressed as

$$i_{\rm z1} = -i_{\rm z2} = \frac{U_{\rm dc}(m_1 - m_2)}{6\omega(L_1 + L_2)}\sin(3\omega t). \tag{4}$$

For PTLIs, a phase current causes the NPP imbalance only when the phase is clamped to the neutral-point. The reference voltage of TLI-k is calculated as $v_{xk} = v_x + v_{{\rm cm}k}$. From (1)–(4), the average neutral current of PTLIs in one period [17] is

$$i_{\rm o} = -\sum_{k=1,2}\sum_{x={\rm a,b,c}}\left(\frac{1}{2}i_x|v_x + v_{{\rm cm}k}| + i_{{\rm z}k}|v_x + v_{{\rm cm}k}|\right). \tag{5}$$

Obviously, the existence of ZSCC has an undeniable effect on the neutral current, which can further affect NPP. From Fig. 1, the NPP of PTLIs can be expressed as

$$u_{\rm o} = \frac{u_{\rm cH} - u_{\rm cL}}{2} = \frac{1}{2C}\int i_{\rm o}{\rm d}t + U_{\rm o} \tag{6}$$

where $u_{\rm cH}$, $u_{\rm cL}$, and C are the voltages and capacitance of $C_{\rm H}$ and $C_{\rm L}$, $U_{\rm o}$ is the initial NPP due to the dc bias of $u_{\rm cH}$ and $u_{\rm cL}$.

Equation (6) shows that the NPP has an ac-imbalance due to the ac fluctuation of the neutral current and a dc-imbalance due to the dc bias of the capacitor voltages. The essence of NPPC is to generate a desired NCC to simultaneously eliminate the dc and ac imbalances [17]. The NCC can be calculated as

$$i_{\rm NCC} = -2Cu_{\rm o}/T_{\rm s} \tag{7}$$

where $T_{\rm s}$ is the switching period.

III. ZSVI Methods for PTLIs Considering ZSCC

The NPPC of PTLIs has to consider the effect of ZSCC. The traditional ZSVI method [16] designed for a single TLI does not consider ZSCC and cannot be directly applied to PTLIs. With the consideration of ZSCC, the independent ZSVI method [17] is extended to PTLIs, treating the PTLIs as two three-phase TLIs. Besides, the PTLIs is proposed to be treated as one six-phase TLI and the uniform ZSVI method is designed to obtain one optimal ZSV of PTLIs to balance NPP.

A. Independent ZSVI Method

The independent ZSVI method injects two ZSVs into the two TLIs separately. The average neutral current of TLI-k is

$$i_{{\rm o}k} = 3i_{{\rm z}k} - \sum_{p=1,2,3}(|v_{pk} + v_{{\rm o}k}|i_{pk}) \tag{8}$$

where $v_{{\rm o}k}$ is the injected ZSV of TLI-k, v_{1k}, v_{2k}, v_{3k} are the reference voltages of TLI-k sorted from small to large, i_{1k}, i_{2k}, i_{3k} are the corresponding phase currents.

From (8), for different $v_{{\rm o}k}$ values, it is necessary to consider ZSCC to analyze the relationship between $i_{{\rm o}k}$ and $v_{{\rm o}k}$.

1) For $v_{{\rm o}k}\leq$-v_{3k}, $i_{{\rm o}k}$ can be expressed as

$$i_{{\rm o}k} = v_{1k}i_{1k} + v_{2k}i_{2k} + v_{3k}i_{3k} + 3v_{{\rm o}k}i_{{\rm z}k} + 3i_{{\rm z}k}. \tag{9}$$

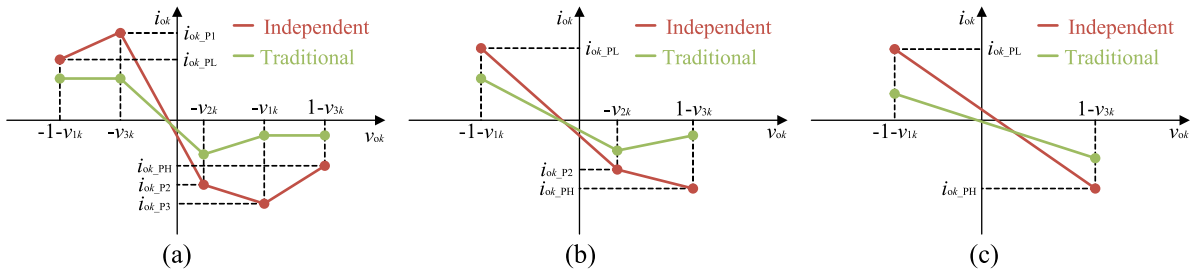

Fig. 2. Relationship between i_{ok} and v_{ok} for the independent and traditional ZSVI methods. (a) Case 1. (b) Case 2. (c) Case 3.

2) For $-v_{3k} \le v_{ok} \le -v_{2k}$, i_{ok} can be expressed as

$$i_{ok} = v_{1k}i_{1k} + v_{2k}i_{2k} - v_{3k}i_{3k} - 2v_{ok}i_{3k} + 3v_{ok}i_{zk} + 3i_{zk}. \quad (10)$$

3) For $-v_{2k} \le v_{ok} \le -v_{1k}$, i_{ok} can be expressed as

$$i_{ok} = v_{1k}i_{1k} - v_{2k}i_{2k} - v_{3k}i_{3k} + 2v_{ok}i_{1k} - 3v_{ok}i_{zk} + 3i_{zk}. \quad (11)$$

4) For $v_{ok} \ge -v_{1k}$, i_{ok} can be expressed as

$$i_{ok} = -v_{1k}i_{1k} - v_{2k}i_{2k} - v_{3k}i_{3k} - 3v_{ok}i_{zk} + 3i_{zk}. \quad (12)$$

From (9)–(12), it can be seen that the relationship between i_{ok} and v_{ok} is piecewise linear, and three key points P1, P2, P3, the neutral currents of which are $i_{ok\cdot P1}$, $i_{ok\cdot P2}$, $i_{ok\cdot P3}$, can be calculated when the ZSVs are $-v_{3k}$, $-v_{2k}$, $-v_{1k}$, respectively.

To avoid overmodulation, there is a range restriction $[-1-v_{1k}, 1-v_{3k}]$ for v_{ok}. Due to the restriction, two boundary points PL and PH, the ZSVs of which are $-1-v_{1k}$ and $1-v_{3k}$, can be calculated for different modulation indexes. The relationship curve between i_{ok} and v_{ok} can be divided into three cases.

Case 1: When $v_{3k}-v_{1k}<1$, the corresponding neutral currents of PL and PH, $i_{ok\cdot PL}$ and $i_{ok\cdot PH}$, are calculated using (9) and (12), and the relationship curve includes four-line segments.

Case 2: When $v_{3k}-v_{1k} \ge 1$ and $-1-v_{1k} < -v_{2k} < 1-v_{3k}$, $i_{ok\cdot PL}$ and $i_{ok\cdot PH}$ are calculated using (10) and (11), and the relationship curve includes two-line segments.

Case 3: When $v_{3k}-v_{1k} \ge 1$ and $-v_{2k} \ge 1-v_{3k}$ or $-v_{2k} \le -1-v_{1k}$, $i_{ok\cdot PL}$ and $i_{ok\cdot PH}$ are calculated using (10) or (11), and the relationship curve includes one line segment.

The process of the traditional ZSVI method is similar to that of the independent ZSVI method. The difference is that the traditional ZSVI method does not consider the existence of ZSCC, which means i_{zk} is 0 in the above process, so the final calculated ZSV is inaccurate. The comparison between the traditional ZSVI method and the independent ZSVI method is shown in Fig. 2.

B. Uniform ZSVI Method

The uniform ZSVI method only injects one ZSV into the PTLIs. At this time, the average neutral current of PTLIs is

$$i_o = -\sum_{q=1,2,3,4,5,6} (|v_q + v_o| i_q) \quad (13)$$

TABLE I
PIECEWISE LINEAR RELATIONSHIP FOR UNIFORM ZSVI

Zero-sequence voltage	Average neutral current
$v_o \le -v_6$	$v_1i_1+v_2i_2+v_3i_3+v_4i_4+v_5i_5+v_6i_6$
$-v_6 \le v_o \le -v_5$	$v_1i_1+v_2i_2+v_3i_3+v_4i_4+v_5i_5-v_6i_6-2v_oi_6$
$-v_5 \le v_o \le -v_4$	$v_1i_1+v_2i_2+v_3i_3+v_4i_4-v_5i_5-v_6i_6-2v_o(i_5+i_6)$
$-v_4 \le v_o \le -v_3$	$v_1i_1+v_2i_2+v_3i_3-v_4i_4-v_5i_5-v_6i_6-2v_o(i_4+i_5+i_6)$
$-v_3 \le v_o \le -v_2$	$v_1i_1+v_2i_2-v_3i_3-v_4i_4-v_5i_5-v_6i_6+2v_o(i_1+i_2)$
$-v_2 \le v_o \le -v_1$	$v_1i_1-v_2i_2-v_3i_3-v_4i_4-v_5i_5-v_6i_6+2v_oi_1$
$v_o \ge -v_1$	$-v_1i_1-v_2i_2-v_3i_3-v_4i_4-v_5i_5-v_6i_6$

where v_o is the injected ZSV of PTLIs, v_1, v_2, v_3, v_4, v_5, v_6 are the reference voltages of TLI-1 and TLI-2 sorted from small to large, i_1, i_2, i_3, i_4, i_5, i_6 are the corresponding phase currents.

From (13), for different v_o values, the relationship between i_o and v_o can be analyzed in detail, as shown in Table I. The relationship between i_o and v_o is also piecewise linear, and six key points P1, P2, P3, P4, P5, and P6 can be determined when the ZSVs are $-v_6$, $-v_5$, $-v_4$, $-v_3$, $-v_2$, $-v_1$, respectively. And, the corresponding neutral currents $i_{o\cdot P1}$, $i_{o\cdot P2}$, $i_{o\cdot P3}$, $i_{o\cdot P4}$, $i_{o\cdot P5}$, $i_{o\cdot P6}$ are calculated according to Table I.

Similarly, to avoid overmodulation, a range restriction $[-1-v_1, 1-v_6]$ for v_o determines that there are also two boundary points PL and PH, the ZSVs of which are $-1-v_1$ and $1-v_6$. For different modulation indexes, the average neutral currents $i_{o\cdot PL}$ and $i_{o\cdot PH}$ can be calculated from Table I, and six cases of the relationship curve between i_o and v_o exist.

Case 1: When $v_6-v_1<1$, the relationship curve includes seven-line segments, as shown in Fig. 3(a).

Case 2: When $v_6-v_1 \ge 1$ and $-1-v_1 < -v_5 < -v_4 < -v_3 < -v_2 < 1-v_6$, the relationship curve includes five line segments, as shown in Fig. 3(b).

Case 3: When $-v_6 \le -1-v_1 < -v_5 < -v_4 < -v_3 < 1-v_6 \le -v_2$ or $-v_5 \le -1-v_1 < -v_4 < -v_3 < -v_2 < 1-v_6 \le -v_1$, the relationship curve includes four line segments, as shown in Fig. 3(c).

Case 4: When $-v_5 \le -1-v_1 < -v_4 < -v_3 < 1-v_6 \le -v_2$, the relationship curve includes three line segments, as shown in Fig. 3(d).

Case 5: When $-v_5 \le -1-v_1 < -v_4 < 1-v_6 \le -v_3$ or $-v_4 \le -1-v_1 < -v_3 < 1-v_6 \le -v_2$ the relationship curve includes two line segments, as shown in Fig. 3(e).

Case 6: When $-v_5 \le -1-v_1 < 1-v_6 \le -v_4$ or $-v_4 \le -1-v_1 < 1-v_6 \le -v_3$ or $-v_3 \le -1-v_1 < 1-v_6 \le -v_2$, the relationship curve includes one line segment, as shown in Fig. 3(f).

The optimal ZSV is calculated through interpolation [16]. By finding, which linear segment i_{NCC} locates in, two segment

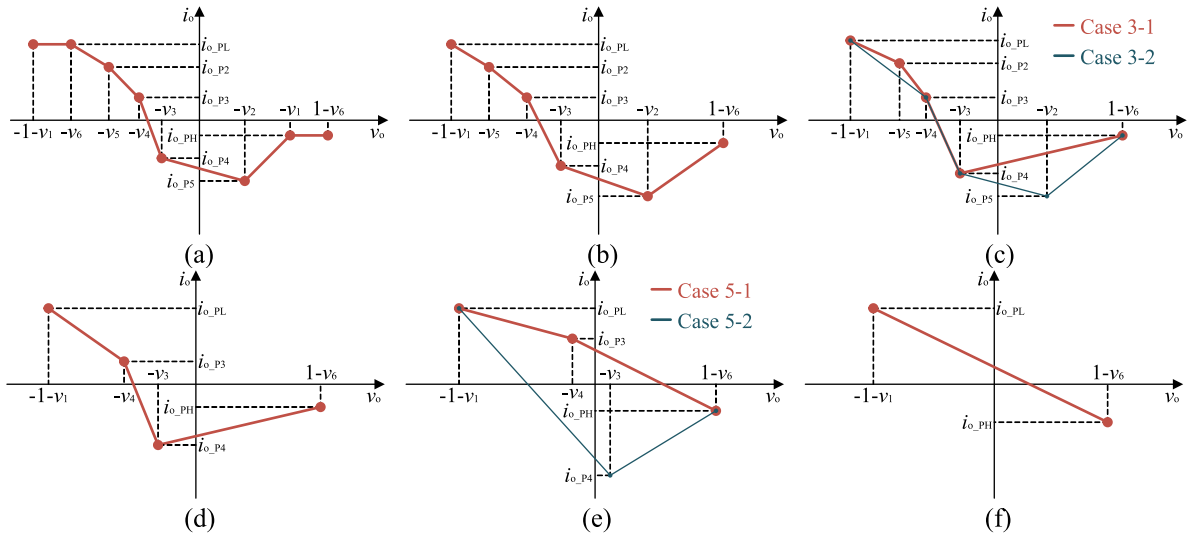

Fig. 3. Relationship between i_o and v_o in different cases. (a) Case 1. (b) Case 2. (c) Case 3. (d) Case 4. (e) Case 5. (f) Case 6.

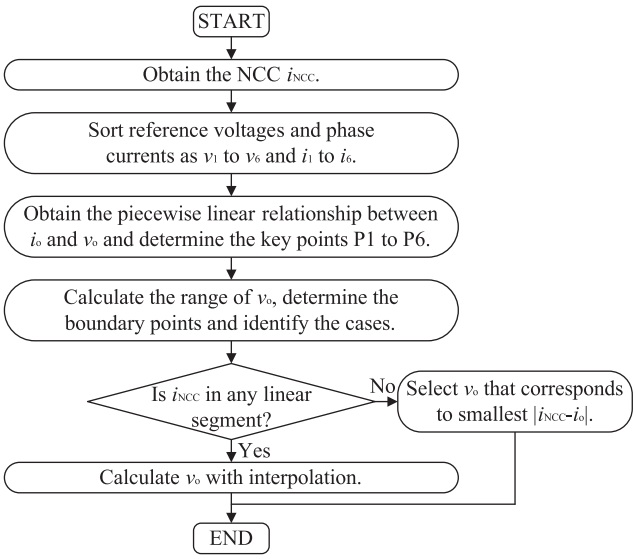

Fig. 4. Flowchart of the uniform ZSVI method for PTLIs.

points are determined, and the optimal ZSV is calculated. It is noted that any line segment can be selected when i_{NCC} is located in multiple linear segments, while the average neutral current closest to i_{NCC} is selected to calculate the optimal ZSV when i_{NCC} is not located in any linear segment. The flowchart of the uniform ZSVI method for PTLIs is shown in Fig. 4, and the process of the independent ZSVI method is similar.

IV. Full-Range and High-Dynamic Control of NPP

A. MWD Method

For PTLIs, the ZSVI method cannot completely eliminate the ac-imbalance of NPP when the modulation index is high [17]. To achieve NPPC in full range, the PTLIs is also treated as one six-phase TLI and the MWD method is designed. All phases of PTLIs can switch between the positive, neutral-point, and negative of the dc-bus in one switching period, and the zero-duty cycle of each phase can be reduced and set to the desired value [19]. Besides, to maintain the switching loss and waveform distortion of PTLIs under reasonable limits, it is necessary to reduce the number of phases switching between three voltage levels in each switching period to the minimum. The flowchart of the MWD method for PTLIs is shown in Fig. 5 and the specific process is as follows.

1) Obtain the NCC i_{NCC}.
2) The ZSV -$(v_1+v_6)/2$ is injected to extend the linear modulation region [19]. For simplicity, the reference voltage of TLI-k after ZSVI is still represented as v_{xk}.
3) Calculate i_{o} with (5), sort subneutral currents from small to large as $i_{\mathrm{o\_n1}}$, $i_{\mathrm{o\_n2}}$, $i_{\mathrm{o\_n3}}$, $i_{\mathrm{o\_n4}}$, $i_{\mathrm{o\_n5}}$, $i_{\mathrm{o\_n6}}$, and define the corresponding zero duty cycles and phase currents as $d_{\mathrm{o\_n1}}$, $d_{\mathrm{o\_n2}}$, $d_{\mathrm{o\_n3}}$, $d_{\mathrm{o\_n4}}$, $d_{\mathrm{o\_n5}}$, $d_{\mathrm{o\_n6}}$ and i_{n1}, i_{n2}, i_{n3}, i_{n4}, i_{n5}, i_{n6}. It is noted that the x-phase subneutral current of TLI-k is (1-$|v_{xk}|$)i_{xk}.
4) According to i_{o} and i_{NCC}, the phases commutating between three voltage levels are selected and the zero duty cycles are modified, which can be divided into three cases.
Case A. $i_{\mathrm{o}} = i_{\mathrm{NCC}}$: In this case, the average neutral current generated by PTLIs can compensate for the imbalance of NPP, so the modulation waves of all phases are not decomposed.
Case B. $i_{\mathrm{o}} < i_{\mathrm{NCC}}$: In this case, it is necessary to increase i_{o} making it equal to i_{NCC}. Therefore, some of the phases with negative contribution to i_{o} have to commutate between three voltage levels. The phase with the most negative contribution to i_{o} is taken as an example. First, it is important to determine whether the phase can be decomposed according to the value of $i_{\mathrm{o\_n1}}$. If $i_{\mathrm{o\_n1}}<0$, the phase can be decomposed and i_{o} can increase after decomposition. On the contrary, if $i_{\mathrm{o\_n1}}\geq 0$, the phase

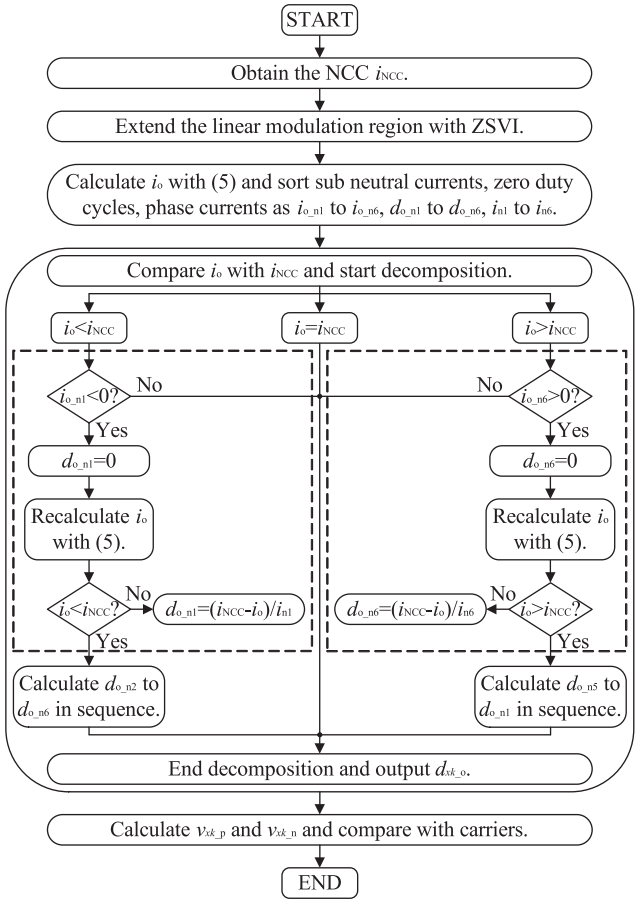

Fig. 5. Flowchart of the MWD method for PTLIs.

cannot be decomposed because i_o cannot increase after decomposition. Then, assuming the zero-duty cycle of the phase is completely decomposed, i_o is recalculated and compared with i_{NCC}. If i_o is still less than i_{NCC}, the zero-duty cycle remain at zero. Otherwise, the zero-duty cycle is recalculated. Finally, the corresponding phases from i_{o_n1} to i_{o_n6} are decomposed in sequence and the new zero duty cycle d_{xk_o} is obtained.

Case C. $i_o > i_{NCC}$: In this case, it is necessary to decrease i_o making it equal to i_{NCC}. Therefore, some of the phases with positive contribution to i_o have to commutate between three voltage levels. The phase with the most positive contribution to i_o is taken as an example. First, it is important to determine whether the phase can be decomposed according to the value of i_{o_n6}. If $i_{o\_n6}>0$, the phase can be decomposed and i_o can decrease after decomposition. On the contrary, if $i_{o\_n6}\leq 0$, the phase cannot be decomposed because i_o cannot decrease after decomposition. Then, assuming the zero-duty cycle of the phase is completely decomposed, i_o is recalculated and compared with i_{NCC}. If i_o is still greater than i_{NCC}, the zero-duty cycle remain at zero. Otherwise, the zero-duty cycle is recalculated. Finally, the corresponding phases from i_{o_n6} to i_{o_n1} are decomposed in sequence and d_{xk_o} is obtained.

5) The positive and negative reference voltages, v_{xk_p} and v_{xk_n}, are calculated using (14) and compared with carriers to generate gate signals

$$\begin{cases} v_{xk\_p} = \frac{1}{2}\left(1 + v_{xk} - d_{xk\_o}\right) \\ v_{xk\_n} = \frac{1}{2}\left(1 - v_{xk} - d_{xk\_o}\right) \end{cases}. \tag{14}$$

B. ONCCE Method

It can be seen that the implementation of the above ZSVI and MWD methods requires an accurate NCC. Commonly, the NCC is calculated using (7) or measured by hardware. However, the system cost greatly increase due to additional hardware. Besides, there are some nonideal factors such as parameter differences, nonlinearities, and external uncertainties that can affect NCC and lead to the considerable discrepancy between the calculated value using (7) and the actual value of NCC. An inaccurate NCC can significantly decrease the dynamic performance of NPPC. To quickly and accurately obtain the desired NCC and improve the dynamic performance of NPPC, an ONCCE method based on "P+NDOB" is presented. All nonideal factors are regarded as the total disturbance, estimated by the NDOB, and rejected by the feedforward compensation. The concept of the total disturbance and its estimation and rejection was first introduced in [23]. The fundamental idea is to lump various known and unknown quantities that affect the system performance as a total disturbance. Therefore, the control problem is transformed to that of estimation and rejection of the total disturbance.

The calculation of NCC using (7) assumes the accurate value of C is available, which may not be the truth in practice. In order to calculate an accuracy NCC, the capacitance variation must be considered, and a more complete model can be rebuilt

$$2C\frac{\mathrm{d}u_o}{\mathrm{d}t} = i_{NCC} - 2\Delta C\frac{\mathrm{d}u_o}{\mathrm{d}t} \tag{15}$$

where ΔC is the capacitance variation.

In addition to the capacitance variation, some nonlinearities and external uncertainties in PTLIs can also affect NCC. Taking all these factors into account, the total disturbance i_d is defined as

$$i_d = -2\Delta C\frac{\mathrm{d}u_o}{\mathrm{d}t} + i_{dn} + i_{du} \tag{16}$$

where i_{dn} and i_{du} are the effects of nonlinearities and external uncertainties on i_{NCC}, respectively.

Therefore, (17) can be obtained from (15) and (16)

$$\frac{\mathrm{d}u_o}{\mathrm{d}t} = \frac{1}{2C}i_{NCC} + \frac{1}{2C}i_d. \tag{17}$$

The NDOB can be designed as

$$\begin{cases} \frac{\mathrm{d}z}{\mathrm{d}t} = -\frac{1}{2C}l(u_o)z - l(u_o)\left[\frac{1}{2C}p(u_o) + \frac{1}{2C}i_{NCC}\right] \\ i_{de} = z + p(u_o) \end{cases} \tag{18}$$

where z, $p(u_o)$, and $l(u_o)$ are the internal state variable, nonlinear function to be designed, and gain function, i_{de} is the estimated

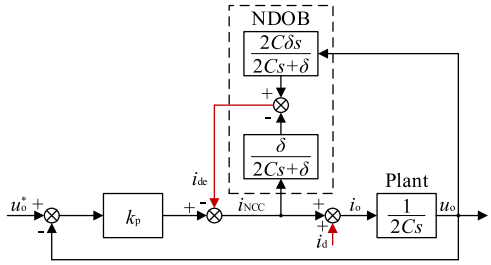

Fig. 6. Block diagram of the ONCCE method.

value of the total disturbance. Besides, the relationship between $l(u_o)$ and $p(u_o)$ can be expressed as $l(u_o) = \partial p(u_o)/\partial u_o$.

To make the error between i_{de} and i_d converge quickly, $l(u_o) = \delta$ (δ>0) is selected [10]. Performing Laplace transform on (18), the transfer function of NDOB can be obtained as

$$i_{de} = \frac{2C\delta s}{2Cs+\delta}u_o(s) - \frac{\delta}{2Cs+\delta}i_{NCC}(s). \tag{19}$$

Besides, the transfer function of the controlled plant is a typical integral link, and a proportional regulator can be adopted as the controller based on the internal principle [24]. Fig. 6 is the block diagram of the ONCCE method. In the figure, the superscript "$*$" represents the reference value, and k_p is the proportional coefficient. Then, the transfer function of the close-loop control system can be obtained as

$$u_o(s) = \frac{k_p}{2Cs+k_p}u_o^*(s) + \frac{2Cs}{(2Cs+\delta)(2Cs+k_p)}i_d(s). \tag{20}$$

It can be seen that $u_o(s)/u_o^*(s)$ is a first-order inertial link, the bandwidth frequency of which is $k_p/2C$. Obviously, with the increase of k_p, the bandwidth frequency increases, and the dynamic performance is improved. But, k_p cannot be too large to prevent noise from being amplified. Besides, the magnitude diagrams of $u_o(s)/i_d(s)$ with k_p and δ when the disturbance frequency is 1 Hz, 300 Hz, and 2000 Hz are shown in Fig. 8. It can be seen that the magnitudes of $u_o(s)/i_d(s)$ for different disturbance frequencies decrease with the increase of k_p and δ, especially when the disturbance frequency is in the low frequency band. In the middle and high frequency bands, the magnitude is already very small. The small magnitude means that the influence of disturbance on the NPP is weakened and the accuracy of NCC is improved. Therefore, considering the dynamic performance of NPPC and the accuracy of NCC, k_p and δ can be chosen as 10 and 1, respectively.

C. Proposed Full-Range and High-Dynamic Control Method

Although the MWD method can achieve the full-range NPPC for PTLIs, it can increase switching losses and deteriorate harmonic characteristics due to the three-level switching of some phases in one switching period. Therefore, it is desirable to perform the MWD method only when the ZSVI method cannot balance NPP. In addition, the ZSVs of TLI-1 and TLI-2 calculated by the independent ZSVI method may be inconsistent, which can lead to an increase of ZSCC and reduce the stability and efficiency of PTLIs. The uniform ZSVI method injects the same ZSV to TLI-1 and TLI-2 and achieves NPPC without affecting ZSCC, which is more attractive to be combined with the MWD method for PTLIs. Therefore, only the uniform ZSVI is used when it can effectively balance NPP, and the "uniform ZSVI + MWD" is used when the NPP is uncontrolled by the uniform ZSVI. The switching process is achieved by setting activation bands. There are two activation bands $[u_{obL}, u_{obH}]$ and $[-u_{obH}, -u_{obL}]$, where u_{obH} and u_{obL} are defined as upper and lower limits, respectively. When u_o is in any activation band, the "uniform ZSVI + MWD" is performed to achieve NPPC.

Fig. 8 shows the implementation of the proposed method for NPPC of PTLIs. The control block diagram and flowchart of the proposed method are shown, as Fig. 8(a) and (b), respectively. The proposed method can be divided into three parts: 1) ONCCE, 2) uniform ZSVI, and 3) MWD. The ONCCE is implemented to obtain an accuracy NCC for the uniform ZSVI and MWD to achieve the high-dynamic NPPC. The uniform ZSVI is implemented to calculate the optimal ZSV. The MWD is implemented based on the injection of the optimal ZSV to achieve the full-range NPPC. According to the value of NPP, the proposed method performs "uniform ZSVI + MWD" or "uniform ZSVI". Finally, the CBPWM is used to compare carriers and reference voltages to generate switching signals.

TABLE II
EXPERIMENTAL PARAMETERS

Symbol	Quantity	Value
U_{dc}	DC-bus voltage	800 V
C_H, C_L	DC-link capacitor	1.14 mF
L_1, L_2	Common-mode inductor	90 μH
R	Load resistance	1 Ω
T_s	Switching period	100 μs
f_r	Fundamental frequency	100 Hz

V. EXPERIMENTAL RESULTS

An experimental prototype of the PTLIs has been built to verify the effectiveness of the proposed method. Fig. 9 shows the experimental platform, which consists of a dc source, a digital controller, a main power circuit, a three-phase resistive load, and some dc capacitors and common-mode inductors. The digital controller adopts the combination of the digital signal processor TMS320F28346 and the field programmable gate array EP3C80F484I7. The insulated-gate bipolar transistor module of FF1000R17IE4 from Infineon is used for the main power circuit. The rated power of the PTLIs is 500 kW, and the experimental parameters are shown in Table II.

Figs. 10 and 11 show the experimental results of the traditional, independent and uniform ZSVI methods when m is 0.8. As shown in Fig. 10, when there is no original ZSCC in the PTLIs, all three methods can effectively balance NPP, and the NPP amplitudes of the three methods are 3.1 V, 4.7 V, and 2.1 V, respectively. As shown in Fig. 11, when the original ZSCC, the amplitude of which is about 34.6 A, exists in the PTLIs, the traditional ZSVI has an ac-imbalance of NPP, the amplitude of which is about 17.5 V. The independent ZSVI

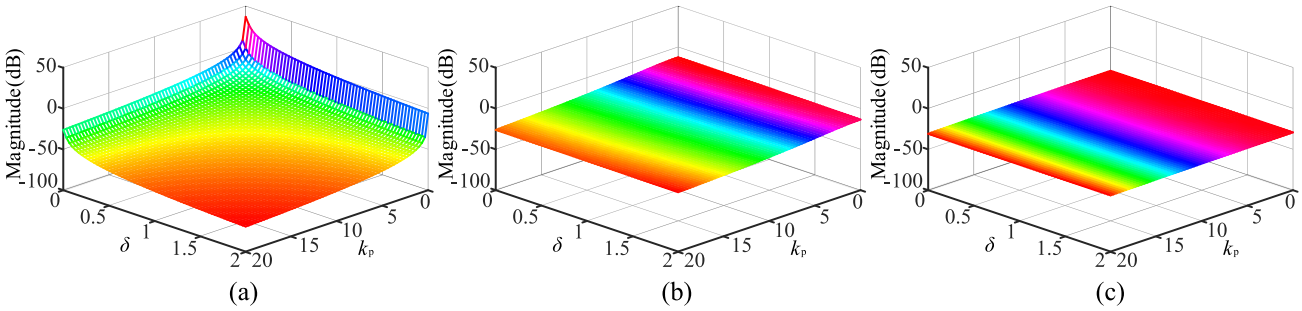

Fig. 7. Magnitude diagrams of $u_o(s)/i_d(s)$ with k_p and δ when the disturbance frequency is (a) 1 Hz, (b) 300 Hz, and (c) 2000 Hz.

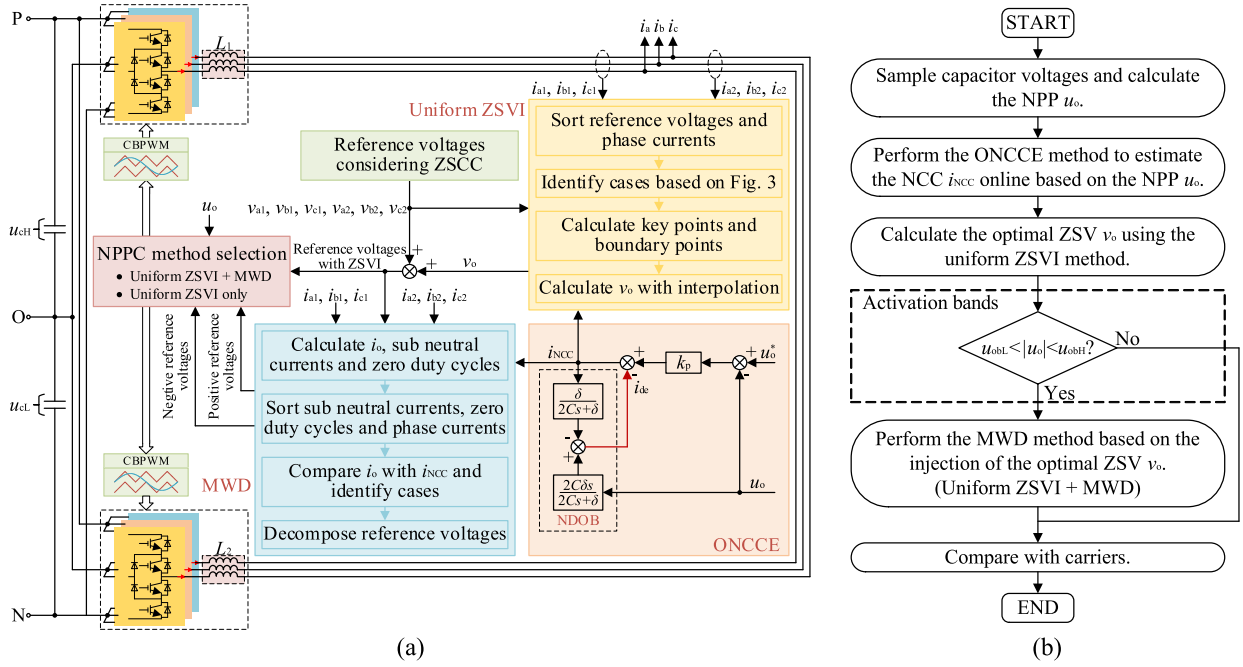

Fig. 8. Implementation of the proposed method. (a) Control block diagram. (b) Flowchart.

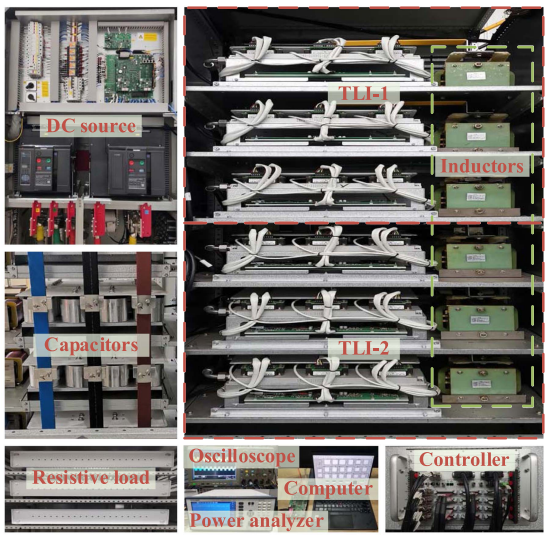

Fig. 9. Experimental platform of the PTLIs.

and uniform ZSVI can still balance NPP, the NPP amplitudes of which are 5.2 V and 2.3 V. It can be seen that the traditional ZSVI cannot suppress the ac-imbalance of NPP due to the lack of consideration for ZSCC while the independent ZSVI will increase ZSCC and distort phase currents of two TLIs due to the injection of two different ZSVs. Therefore, the uniform ZSVI can satisfactorily control the ac-imbalance of NPP and balance the voltages of C_H and C_L without affecting ZSCC.

Figs. 12 and 13 show the experimental results of the uniform ZSVI, MWD and proposed method under different modulation indexes. The original ZSCC still exists in the PTLIs. From Fig. 12, it can be seen when m is 1, all three methods can balance NPP, and the NPP amplitudes of the three methods are 3.9 V, 3.2 V, and 2.4 V, respectively. However, the MWD significantly increases the switching loss due to some three-level switching states of the phase voltages for TLI-1 and TLI-2. The uniform ZSVI and proposed method will not generate extra switching actions, and the amplitude of NPP for the proposed method is

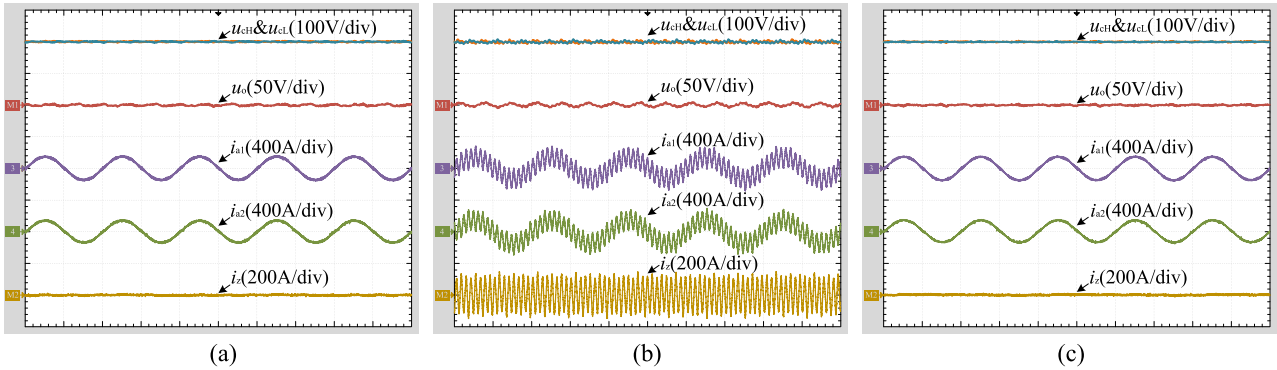

Fig. 10. Experimental results without the original ZSCC ($m = 0.8$). (a) Traditional ZSVI. (b) Independent ZSVI. (c) Uniform ZSVI. (Time scale: 5 ms/div.)

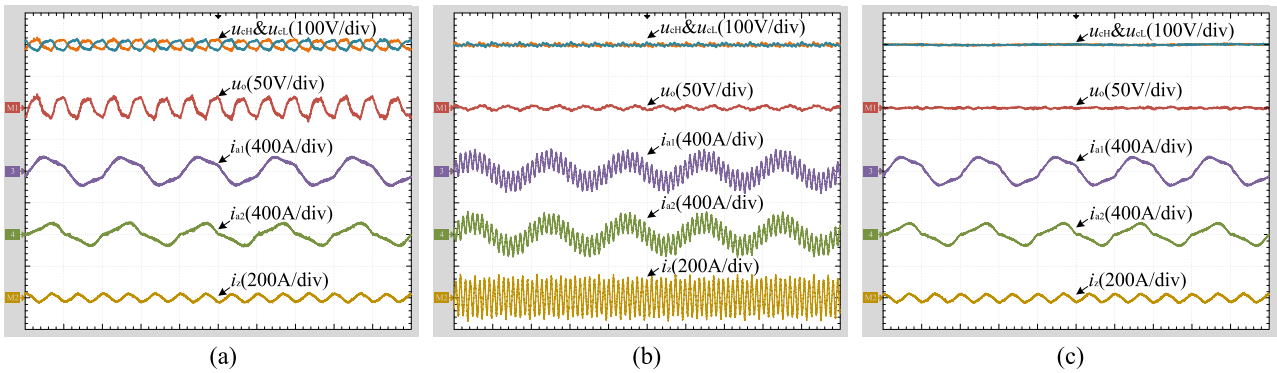

Fig. 11. Experimental results with the original ZSCC ($m = 0.8$). (a) Traditional ZSVI. (b) Independent ZSVI. (c) Uniform ZSVI. (Time scale: 5 ms/div.)

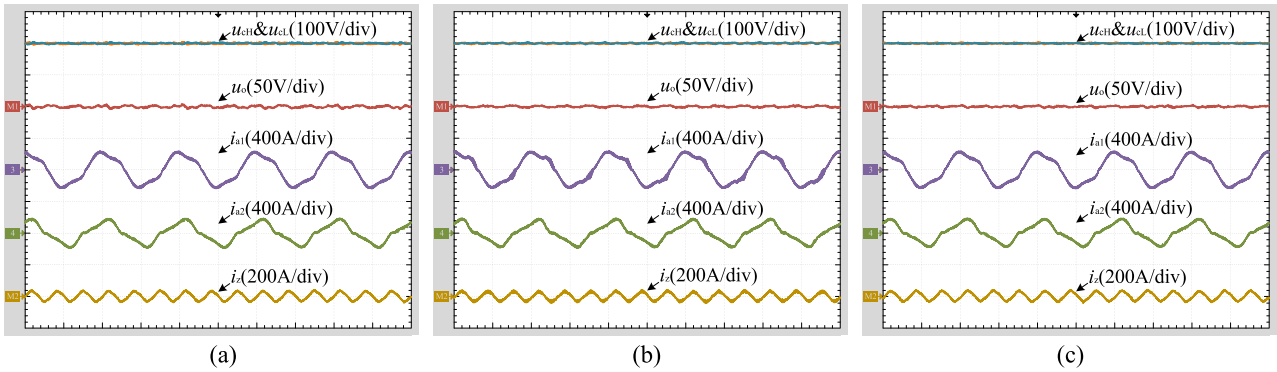

Fig. 12. Experimental results ($m = 1$). (a) Uniform ZSVI. (b) MWD. (c) Proposed method. (Time scale: 5 ms/div.)

smaller due to a more accurate NCC compared with the uniform ZSVI. From Fig. 13, it can be seen when m is 1.15, the NPP amplitudes of the three methods are 12.4 V, 3.4 V, and 3.7 V, respectively. The results show when the PTLIs operates at a high modulation index, the uniform ZSVI cannot suppress the ac-imbalance of NPP while the MWD and proposed method can achieve NPPC in full range. Compared with MWD, the proposed method has fewer three-level switching states, so the switching loss is smaller while the harmonic characteristic is better. For the proposed method, the uniform ZSVI based on ONCCE is performed when m is 1, while the "uniform ZSVI + MWD" based on ONCCE is performed when m is 1.15.

The waveforms of the phase voltages u_{a1} and u_{a2} of TLI-1 and TLI-2, as well as the waveform of the line voltage u_{ab} of PTLIs, are shown in Fig. 14. From Fig. 14, when m is 1, only the MWD has three-level switching states among the three methods, the switching loss of which is highest. When m is 1.15, the proposed method and MWD both have extra three-level switching states, but the three-level switching states of the proposed method is fewer, indicating a lower switching loss. Fig. 15 shows the THD

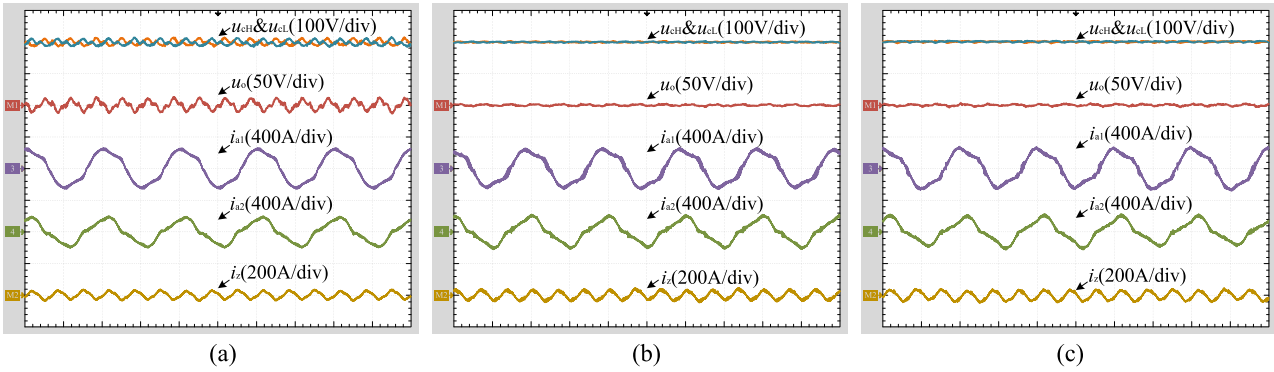

Fig. 13. Experimental results ($m = 1.15$). (a) Uniform ZSVI. (b) MWD. (c) Proposed method. (Time scale: 5 ms/div.)

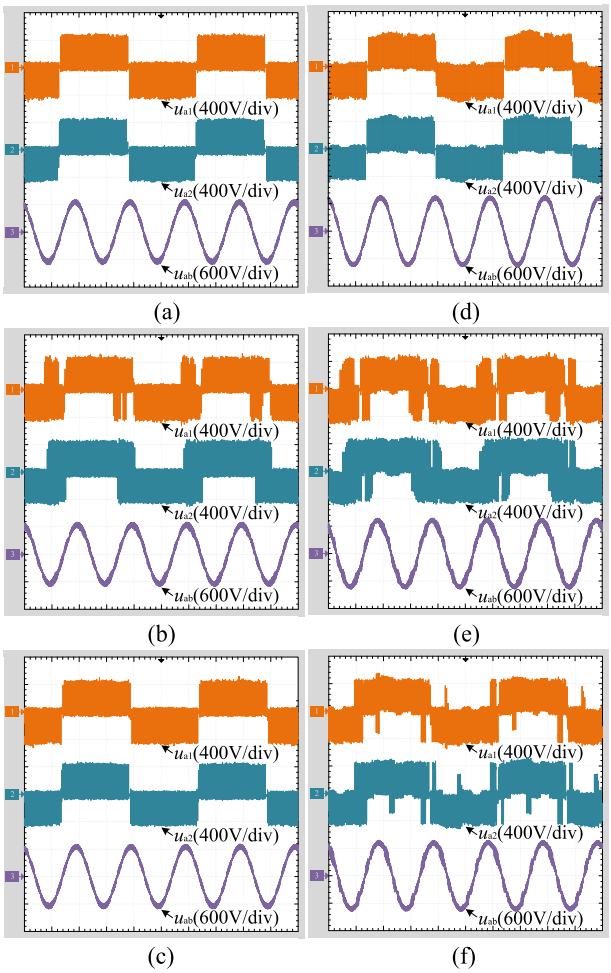

Fig. 14. Experimental results of u_{a1}, u_{a2}, and u_{ab}. (a) Uniform ZSVI ($m = 1$). (b) MWD ($m = 1$). (c) Proposed method ($m = 1$). (d) Uniform ZSVI ($m = 1.15$). (e) MWD ($m = 1.15$). (f) Proposed method ($m = 1.15$). (Time scale: 5 ms/div.)

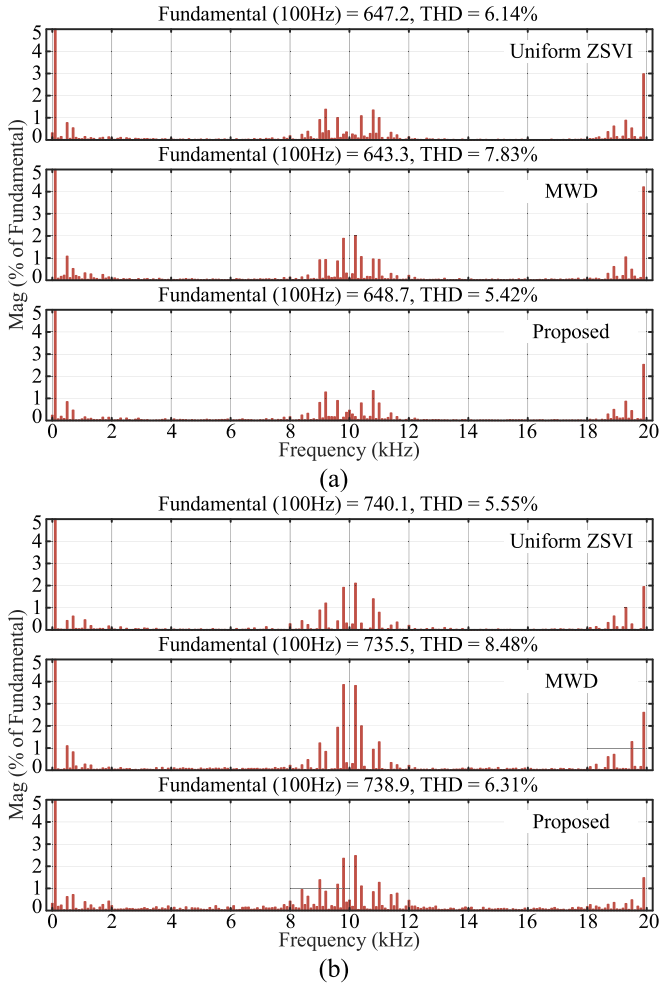

Fig. 15. THD comparison of u_{ab}. (a) m is 1. (b) m is 1.15.

comparison of u_{ab} of the three methods. The results of the three methods are 6.14%, 7.83%, and 5.42% when m is 1, and 5.55%, 8.48%, and 6.31% when m is 1.15, respectively. Compared with the other two methods, the proposed method can achieve the full-range NPPC with better harmonic characteristics.

The power loss and efficiency of the experimental prototype has been measured by the power analyzer Zimmer LMG671. Fig. 16 shows the power loss and efficiency curves for the three methods under different modulation indexes. It can be seen that the MWD has the highest power loss and the lowest efficiency. Compared with the uniform ZSVI, the proposed method has

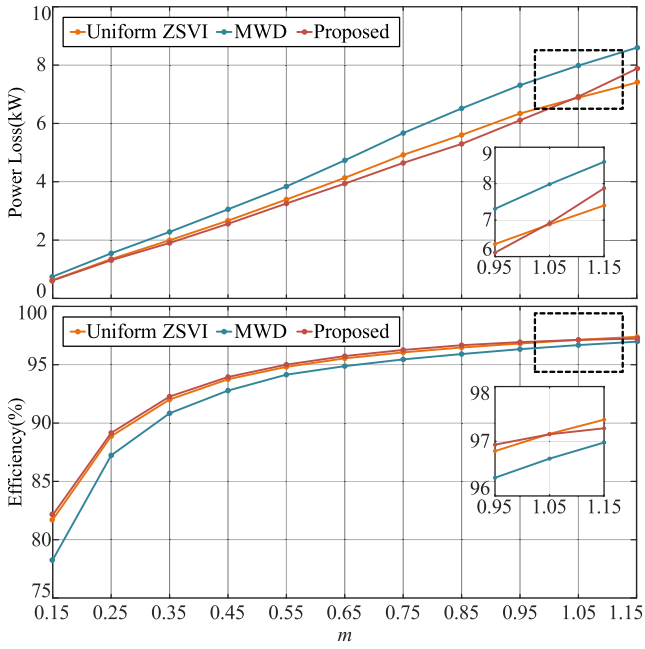

Fig. 16. Comparison of power loss and efficiency.

lower power loss and higher efficiency under most modulation indexes, except for high modulation indexes. Therefore, the power loss and efficiency of the proposed method are optimal under low modulation indexes, while the power loss and efficiency of the proposed method is compromise under high modulation indexes.

Fig. 17 shows the dynamic experimental results of the three methods for NPPC under different modulation indexes. The original difference between u_{cH} and u_{cL} is 200 V, and the dc-imbalance of NPP is 100 V. When m is 1, the balance times of the three methods are 2.8 ms, 4.0 ms, and 1.9 ms, respectively. Although the proposed method only performs "uniform ZSVI" at this time, its balance time is shorter than that of the uniform ZSVI method due to the online estimation of NCC. When m is 1.15, the balance times of the three methods are 6.7 ms, 7.5 ms, and 3.3 ms, respectively. The proposed method performs "uniform ZSVI + MWD" at this time, and its balance time is also the shortest due to the ONCCE method. Therefore, it can be seen that the proposed method has the best dynamic performance of NPPC under different modulation indexes.

To further verify the effectiveness of the ONCCE method, the dynamic experiment of the proposed method is conducted with inaccurate capacitance values of C_H and C_L. For comparison, the proposed method without or with ONCCE is performed under different modulation indexes. The dynamic experiment results with inaccurate capacitance values are shown in Fig. 18. When m is 1, the balance times of the proposed method without and with ONCCE are 4.5 ms and 2.5 ms. When m is 1.15, the balance times of the proposed method without and with ONCCE are 10.6 ms and 4.7 ms. It can be seen that the balance times with ONCCE is shorter than that without ONCCE under different modulation indexes.

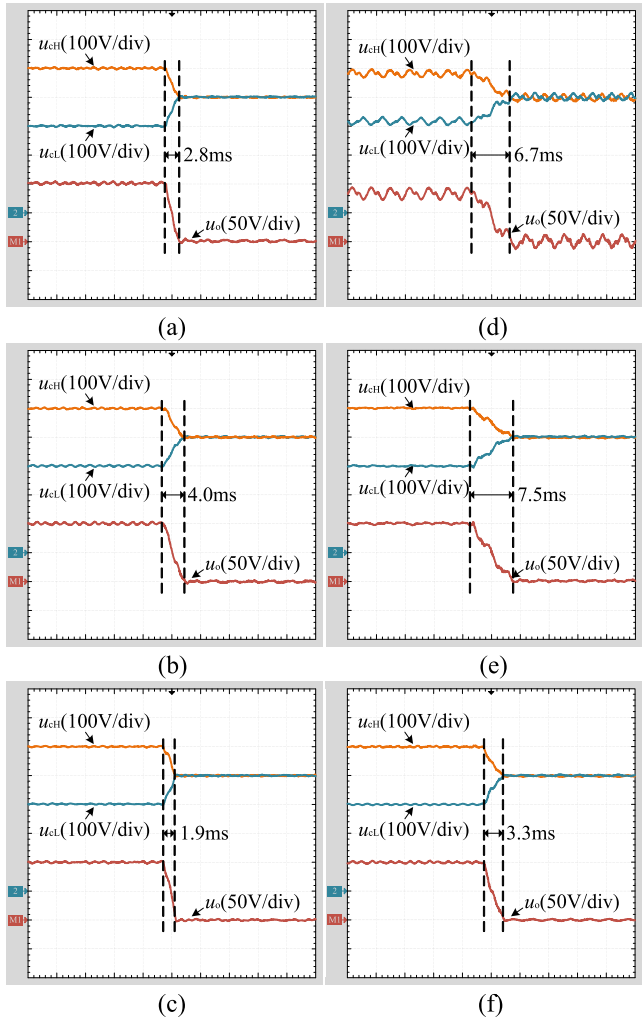

Fig. 17. Dynamic experimental results. (a) Uniform ZSVI ($m = 1$). (b) MWD ($m = 1$). (c) Proposed method ($m = 1$). (d) Uniform ZSVI ($m = 1.15$). (e) MWD ($m = 1.15$). (f) Proposed method ($m = 1.15$). (Time scale: 5 ms/div.)

To verify the performance of the proposed method during modulation index transients, the experimental results when m changes from 0.8 to 1.15 without ZSCC suppression are presented in Fig. 19(a). The experimental waveforms show the NPP can still be well balanced, which proves the effectiveness of the proposed method during modulation index transients. Besides, the dynamic experimental results with ZSCC suppression are presented in Fig. 19(b). The ZSCC suppression method proposed in [10] is adopted. It can be seen that the NPP can remain balanced and the ZSCC can be well suppressed.

VI. Conclusion

This article proposes a full-range and high-dynamic control method of NPP for PTLIs considering ZSCC. The traditional ZSVI method cannot balance NPP when ZSCC exists in PTLIs. The independent ZSVI and uniform ZSCI methods are extended to PTLIs, balancing NPP whether ZSCC exists in PTLIs or not. The independent ZSVI method will increase ZSCC, while the

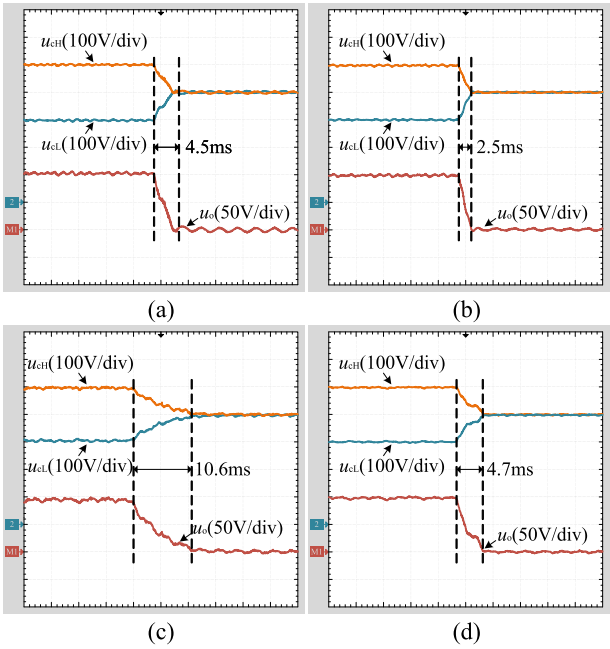

Fig. 18. Dynamic experimental results with inaccurate capacitance values. (a) Without ONCCE ($m = 1$). (b) With ONCCE ($m = 1$). (c) Without ONCCE ($m = 1.15$). (d) With ONCCE ($m = 1.15$). (Time scale: 5 ms/div.)

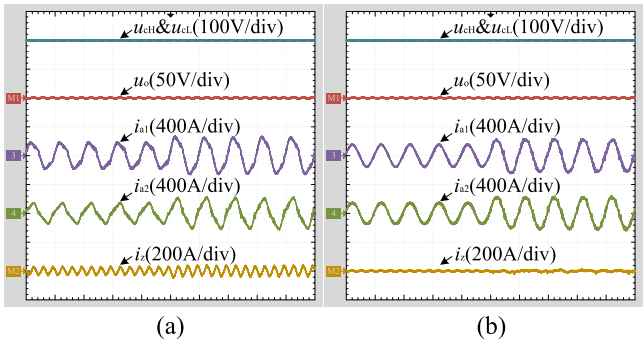

Fig. 19. Dynamic experimental results when m changes from 0.8 to 1.15. (a) Without ZSCC suppression. (b) With ZSCC suppression. (Time scale: 10 ms/div.)

uniform ZSVI method will not. Besides, the MWD method is extended to PTLIs, treating the PTLIs as a multiphase TLI, to achieve the full-range NPPC. The proposed method generally performs the uniform ZSVI, and only activates MWD when necessary, which moderates switching losses and harmonics. The ONCCE method can quickly and accurately obtain the NCC, achieving the high-dynamic NPPC. Since the proposed method is simple and reliable, it can be easily applied to multiple TLIs in parallel.

REFERENCES

[1] X. Zhang and J. Yang, "A robust flywheel energy storage system discharge strategy for wide speed range operation," *IEEE Trans. Ind. Electron.*, vol. 64, no. 10, pp. 7862–7873, Oct. 2017.

[2] W. Wan, S. Duan, C. Chen, and T. Yu, "A hybrid control method for neutral-point voltage balancing in three-level inverters," *IEEE Trans. Power Electron.*, vol. 36, no. 8, pp. 8575–8582, Aug. 2021.

[3] A. Zorig, S. Barkat, and A. Sangwongwanich, "Neutral point voltage balancing control based on adjusting application times of redundant vectors for three-level NPC inverter," *IEEE J. Emerg. Sel. Topics Power Electron.*, vol. 10, no. 5, pp. 5604–5613, Oct. 2022.

[4] A. Tcai, Y. Kwon, S. Pugliese, and M. Liserre, "Reduction of the circulating current among parallel NPC inverters," *IEEE Trans. Power Electron.*, vol. 36, no. 11, pp. 12504–12514, Nov. 2021.

[5] Z. Chen et al., "The tolerance control method based on zero-sequence circulating current suppression for parallel T-type three-level rectifiers," *IEEE J. Emerg. Sel. Topics Power Electron.*, vol. 10, no. 4, pp. 4383–4394, Aug. 2022.

[6] K. Sun, X. Lin, Y. Li, Y. Gao, and L. Zhang, "Improved modulation mechanism of parallel-operated T-type three-level PWM rectifiers for neutral-point potential balancing and circulating current suppression," *IEEE Trans. Power Electron.*, vol. 33, no. 9, pp. 7466–7479, Sep. 2018.

[7] J. Liu, X. Sun, B. Ren, and Q. Zhang, "Dynamic circulating current suppression method for multiple hybrid power parallel grid-connected inverters with model reference adaptive system," *IEEE Trans. Ind. Electron.*, vol. 69, no. 5, pp. 4364–4375, May 2022.

[8] W. Li, X. Zhang, Y. Zhuang, G. Zhang, G. Wang, and D. Xu, "A five-level space vector modulation scheme for parallel operated three-level inverters with reduced line current distortion," *IEEE Trans. Power Electron.*, vol. 35, no. 10, pp. 11235–11249, Oct. 2020.

[9] F. Guo, Z. Ma, F. Diao, Y. Zhao, and P. Wheeler, "Hybrid virtual coordinate-driven CBPWM strategy of three-level T-type NPC converters for electric aircraft propulsion applications," *IEEE Trans. Ind. Electron.*, vol. 71, no. 3, pp. 2309–2319, Mar. 2024, doi: 10.1109/TIE.2023.3266552.

[10] Z. Li, Z. Nie, and S. Ai, "Nonlinear modeling and improved suppression of zero-sequence circulating current for parallel three-level inverters," *IEEE J. Emerg. Sel. Topics Power Electron.*, vol. 11, no. 3, pp. 3036–3049, Jun. 2023.

[11] X. Xing, X. Li, F. Gao, C. Qin, and C. Zhang, "Improved space vector modulation technique for neutral-point voltage oscillation and common-mode voltage reduction in three-level inverter," *IEEE Trans. Power Electron.*, vol. 34, no. 9, pp. 8697–8714, Sep. 2019.

[12] S. Busquets-Monge, J. Bordonau, D. Boroyevich, and S. Somavilla, "The nearest three virtual space vector PWM-a modulation for the comprehensive neutral-point balancing in the three-level NPC inverter," *IEEE Power Electron. Lett.*, vol. 2, no. 1, pp. 11–15, Mar. 2004.

[13] W. Jiang et al., "A novel virtual space vector modulation with reduced common-mode voltage and eliminated neutral point voltage oscillation for neutral point clamped three-level inverter," *IEEE Trans. Ind. Electron.*, vol. 67, no. 2, pp. 884–894, Feb. 2020.

[14] W. Jiang, S. Du, L. Chang, Y. Zhang, and Q. Zhao, "Hybrid PWM strategy of SVPWM and VSVPWM for NPC three-level voltage-source inverter," *IEEE Trans. Power Electron.*, vol. 25, no. 10, pp. 2607–2619, Oct. 2010.

[15] C. Xia, H. Shao, Y. Zhang, and X. He, "Adjustable proportional hybrid SVPWM strategy for neutral-point-clamped three-level inverters," *IEEE Trans. Ind. Electron.*, vol. 60, no. 10, pp. 4234–4242, Oct. 2013.

[16] C. Wang and Y. Li, "Analysis and calculation of zero-sequence voltage considering neutral-point potential balancing in three-level NPC converters," *IEEE Trans. Ind. Electron.*, vol. 57, no. 7, pp. 2262–2271, Jul. 2010.

[17] Z. Dong, C. Wang, K. Cui, Q. Cheng, and J. Wang, "Neutral-point voltage-balancing strategies of NPC-inverter fed dual three-phase ac motors," *IEEE Trans. Power Electron.*, vol. 36, no. 3, pp. 3181–3191, Mar. 2021.

[18] J. Pou et al., "Fast-processing modulation strategy for the neutral-point-clamped converter with total elimination of low-frequency voltage oscillations in the neutral point," *IEEE Trans. Ind. Electron.*, vol. 54, no. 4, pp. 2288–2294, Aug. 2007.

[19] I. López et al., "Modulation strategy for multiphase neutral-point-clamped converters," *IEEE Trans. Power Electron.*, vol. 31, no. 2, pp. 928–941, Feb. 2016.

[20] J. Wang, X. Yuan, K. J. Dagan, and A. Bloor, "Optimal neutral-point voltage balancing algorithm for three-phase three-level converters with hybrid zero-sequence signal injection and virtual zero-level modulation," *IEEE Trans. Ind. Appl.*, vol. 56, no. 4, pp. 3865–3878, Jul./Aug. 2020.

[21] Z. Dong, C. Wang, and Q. Cheng, "A hybrid modulation method with the maximum controllable range of the neutral-point current for three-level NPC," *IEEE Trans. Transp. Electrific.*, vol. 8, no. 4, pp. 4444–4455, Dec. 2022.

[22] Z. Liang, X. Lin, X. Qiao, Y. Kang, and B. Gao, "A coordinated strategy providing zero-sequence circulating current suppression and neutral-point potential balancing in two parallel three-level converters," *IEEE J. Emerg. Sel. Topics Power Electron.*, vol. 6, no. 1, pp. 363–376, Mar. 2018.

[23] J. Han, "From PID to active disturbance rejection control," *IEEE Trans. Ind. Electron.*, vol. 56, no. 3, pp. 900–906, Mar. 2009.
[24] H.-J. Lee, T. Woo, S. Kim, and Y.-D. Yoon, "Improved neutral-point voltage balancing control with time delay compensation and antiwindup loop for a three-level NPC inverter," *IEEE Trans. Ind. Appl.*, vol. 57, no. 5, pp. 4970–4980, Sep. 2021.

Zhongrui Li was born in Shandong Province, China, in 1997. He received the B.S. degree from Zhejiang University, Zhejiang, China, in 2019. He is currently working toward the Ph.D. degree with the State Key Laboratory of Electromagnetic Energy, Naval University of Engineering, Wuhan, China, both in electrical engineering.

His research interests include multilevel converters, multiphase machine drives, and flywheel energy storage system.

Ziling Nie received the B.S. (hons.), M.S., and Ph.D. degrees from Huazhong University of Science and Technology, Wuhan, China, in 1998, 2001, and 2005, respectively.

From 2008 to 2009, he was a Visiting Scholar with the University of Michigan, Ann Arbor, MI, USA. He is currently a Professor with the Naval University of Engineering, Wuhan, China. His current research interests include power electronics and electric drives.

Sheng Ai received the B.S., M.S., and Ph.D. degrees from Naval University of Engineering, Wuhan, China, in 2007, 2009, and 2017, respectively.

From 2018 to 2019, he was a Visiting Scholar with Arizona State University, Tempe, AZ, USA. He is currently a Professor with the Naval University of Engineering, Wuhan, China. His current research interests include power electronics and electric drives.

Jie Xu received the Ph.D. degree in electric engineering from Naval University of Engineering, Wuhan, China, in 2017.

He is currently a Research Associate Professor with the Naval University of Engineering, Wuhan, China. His current research interests include signal processing and power electronics.

Huayu Li received the B.E. degree in automation from Central South University, Changsha, China, in 2012, the M.S. degree in electrical engineering from Naval University of Engineering, Wuhan, China, in 2014, and the Ph.D. degree in electromechanical engineering from Ghent University, Ghent, Belgium, in 2020.

He is currently a Research Associate with the Naval University of Engineering, Wuhan, China. His current research interests include machine parameters identification, direct torque control, and model predictive control.